UNIVERSIDADE DA BEIRA INTERIOR
Ciências

Design and production of sintered ß-Tricalcium phosphate 3D scaffolds for bone tissue regeneration

Carlos Filipe Lopes Santos

Master degree thesis in

Biochemistry

(2nd cycle of studies)

Supervisor: Ilídio Joaquim Sobreira Correia, Ph.D.

Covilhã, June 2011

UNIVERSIDADE DA BEIRA INTERIOR
Ciências

Desenho e produção de estruturas tridimensionais de ß-Tricálcio fosfato sinterizadas para futura aplicação na regeneração óssea

Carlos Filipe Lopes Santos

Dissertação para obtenção do Grau de Mestre em

Bioquímica

(2º ciclo de estudos)

Orientador: Prof. Doutor Ilídio Joaquim Sobreira Correia

Covilhã, Junho de 2011

“For the tenacious, no road is impassable”

- **Spyker**

Acknowledgments

I start by expressing my gratitude to my supervisor, Professor Ilídio Correia, for the opportunity to develop this project, for is boundless support and for his friendship. His commitment to work and perseverance have never ceased to amaze me.

Huge thanks to Luis Lopes, for his massive availability when helping me in the 3D-design. I do believe I found a friend.

I acknowledge to Professor Abílio Silva and to Mr. João Correia from Departamento de Engenharia Electromecânica da Universidade da Beira Interior, for the knowledge and technical support in the making of this project.

I would like to thank to Centro Hospitalar da Cova da Beira for the Computed Tomography data they provided and to Eng. Ana Paula from Centro de Óptica da Universidade da Beira Interior for the help in the Scanning Electron Microscopy images.

To all my group colleagues, thanks for the support in this path of blood, sweat and tears… Thanks for all the knowledge, I've really learned a lot with you guys, and for that I'll always be grateful.

To all my friends, I thank you for the laugh and encouragement… Honestly!

A million-mile-long thanks to dad, mom, little sis and all my family, for your absolute believe. If I've reached so far, it's you I owe…

Finally, I would like to thank to my girlfriend for her colossal patience, for the advices and for always be there when I most needed.

To all… thank you very much!

Abstract

In the past decade, Tissue Engineering has emerged as a promising approach to orthopedic healing. By combining biomaterials, cells and/or growth factors, some Tissue Engineering methodologies have been used in bone or cartilage regeneration. However, the production of an ideal scaffold to support bone tissue regeneration still raises many questions in the scientific community, not only in terms of conceptual design but also in the material selection.

Computer Aided Tissue Engineering allows the design of scaffolds using as template, data from real patient's bodies obtained for example with computed tomography (CT).

The present study describes the characterization of the mechanical and biological properties of the sintered ß-tricalcium phosphate 3D scaffold produced by rapid prototyping based on patient's CT scan data. The scaffolds were characterized by Scanning Electron Microscopy, Fourier transform infrared spectroscopy, X-Ray diffraction and by mechanical tests adapted from C20 ASTM Standards Test Methods. Finally, the cytotoxic profile of the prepared scaffolds was evaluated in vitro by using human osteoblast cells.

The results obtained showed that the scaffolds herein produced have good mechanical properties and are also biocompatible, which is fundamental for its application in a near future as bone substitutes for individualized therapy.

Keywords

ß-Tricalcium phosphate scaffolds, Bone regeneration, Computer Aided Tissue Engineering, Individualized Scaffolds, Rapid Prototyping.

Resumo

Na última década, a Engenharia de Tecidos emergiu como uma abordagem promissora para a resolução de problemas ortopédicos. Utilizando uma combinação de biomateriais, células e/ou factores de crescimento, algumas metedologias da Engenharia de Tecidos têm sido usadas na regeneração do osso ou da cartilagem. No entanto, a produção de suportes ideais para a regeneração óssea ainda suscita muitas dúvidas na comunidade científica, não só em termos de métodos de concepção, mas também na selecção de materiais. A Engenharia de Tecidos Assistida por Computador permite a criação de suportes tendo por base os dados obtidos em exames hospitalares de rotina como sejam, a Tomografia Computorizada.

O presente estudo descreve a caracterização das propriedades mecânicas e biológicas de suportes tridimensionais de ß-Tricálcio fosfato sinterizado, produzidos por prototipagem rápida, baseada em dados reais de Tomografia Computorizada. Os materiais usados no presente trabalho foram caracterizados por Microscopia Eletrónica de Varrimento, Espectroscopia de Infravermelho por Transformada de Fourier, Difração de Raios-X e testes mecânicos baseados na norma *C20 ASTM Standards Test Methods*. Foram ainda semeados osteoblastos humanos na presença dos suportes de ß-Tricálcio fosfato e observada a sua adesão e proliferação celular, após 24 horas. Para além disso, a viabilidade celular foi avaliada através de um ensaio de MTS.

Os resultados obtidos mostraram que os suportes têm boas propriedades mecânicas e biológicas, fundamentais para a sua futura utilização como substitutos ósseos numa terapia personalizada.

Palavras chave

Suportes de ß-Tricálcio fosfato, Regeneração Óssea, Engenharia de Tecidos Assistida por Computador, Suportes Individualizados, Prototipagem Rápida.

Index

Chapter I

Chapter II

Chapter III

Chapter IV

List of Figures

List of Tables

List of Acronyms

2D	Two-dimensional
3D	Three-dimensional
3DP	Three-dimensional printing
BMPs	Bone Morphogenetic Proteins
CAD	Computer Aided Design
CAM	Computer Aided Manufacturing
CATE	Computer Aided Tissue Engineering
CT	Computed Tomography
d90	90% of the particle diameter
DICOM	Digital Imaging and Communications in Medicine
DMEM-F12	Dulbecco's Modified Eagle Medium-F12
ECM	Extracellular Matrix
EDTA	Ethylenediaminetetraacetic acid
EtOH	Ethanol
FBS	Fetal bovine serum
FDM	Fused Deposition Modeling
FTIR	Fourier transform infrared spectroscopy
GF	Growth Factors
K-	Negative Control
K+	Positive Control
MRI	Magnetic Resonance Imaging
MTS	3-(4,5-dimethylthiazol-2-yl)-5-(3carboxymethoxyphenyl)-2-(4-sulfophenyl) -2H-tetrazolium, inner salt
OM	Optical Microscopy
PBS	Phosphate-buffered saline
RGD	Arginine-Glycine-Aspartic acid
RP	Rapid Prototyping
SEM	Scanning Electron Microscopy
SLS	Selective Laser Sintering
STL	Stereolithography
TE	Tissue Engineering
UV	Ultra-violet
XRD	X-Ray diffraction
ß-TCP	ß-Tricalcium phosphate

Chapter I

Introduction

1. Introduction

Degenerative bone diseases and fractures are known to affect millions of people worldwide. Currently, it is expected that by the year 2020 the percentage of persons over 50 years of age affected by bone diseases will double (Sturm et al. 2010).

Bone tissue has a remarkable regenerative capacity, but in cases of patients with limited healing, such as those with diabetes or poor nutrition, its regeneration is very slow and do not suppress the needs in cause. Natural bone regeneration involves the formation of new bone instead of fibrotic tissue, which is common in the regeneration process of other body tissues (Van der Stok et al. 2010). The mechanism of bone restoration is highly regulated and influenced by physiological, cellular and genetic factors (Schindeler et al. 2008).

Nowadays, clinical treatments have been based on replacing the lost bone with autogenous bone grafts, allogeneic banked bone or xenogeneic sources as well as synthetic bone substitutes. However, all of them have a limited degree of structural and functional recovery (Navarro et al. 2008).

In order to overcome these obstacles different studies have been carried out in the area of bone tissue engineering (Sun & Lal 2002). The primary goal of Tissue Engineering (TE) is to produce functional substitutes for damaged tissues (Duan & M. Wang 2010). So far, different three-dimensional (3D) scaffolds have been produced to act as temporary skeleton for new tissue to grow and restore the damaged one (Sun & Lal 2002). Nevertheless, the ideal scaffold is yet to be produced since it must have properties that allow the restoration of native tissue structure and function. Properties like biocompatibility, biodegradability, mechanical characteristics, pore size and surface charge are very important to allow cell adhesion and proliferation, diffusion of nutrients and gases, and subsequently assure the success of tissue regeneration (Williams et al. 2005).

Lately, computer aided technologies and its research tools have been incorporated into TE, creating a new field called Computer Aided Tissue Engineering (CATE) (Sun & Lal 2002; Lacroix et al. 2009). As previously mentioned, a well succeeded bone restoration heavily depends on the structure and mechanical properties of the scaffold, so it is of vital importance to create 3D models suitable to be incorporated in the anatomic defect (Sun & Lal 2002). Additionally, computer aided design (CAD) can contribute to decrease the experimental trials as well as the production time of the scaffold (Krupa et al. 2007).

Scaffold design using individualized patient data allows the production of more accurate and specific models, capable of fitting perfectly into the patient's bone defect. Using today's image acquisition technology, such as Computed Tomography (CT) or Magnetic Resonance Imaging (MRI), it is possible to obtain an accurate 3D anatomic model of the tissue/area of interest (Perera et al. 2010). Based on the data collected in daily routine clinic examinations and using CAD and computer aided manufacturing (CAM) programs, a 3D volume of the tissue can be rendered, and then be used in the production of a patient specific physical model through rapid prototyping (RP) techniques (Perera et al. 2010).

Calcium phosphate based materials are commonly used in biomedical applications because of their osteoconductive and osteoinductive properties (Kondo et al. 2006). Since hydroxyapatite is the major mineral phase present in the bone, it is usually the first selection for scaffold production to be used in bone regeneration (Krupa et al. 2007). Conversely, hydroxyapatite's low biodegradability level is a handicap for bone replacement. In recent studies, β-Tricalcium phosphate (β-TCP) has been used in scaffold production and revealed better results for bone formation and degradation rate, than those obtained for hydroxyapatite (Perera et al. 2010).

The work presented in this thesis describes the design, production and characterization of sintered β-TCP scaffolds for bone tissue regeneration.

1.1. The Bone

1.1.1. Bone Tissue

Bone is a composite material consisting of mineral, matrix, cells and water. Bone tissue is the most rigid of all the connective tissues, a feature largely related with the calcium phosphate (calcium hydroxyapatite) deposited within the bone matrix, although having some level of flexibility due to collagen fibers also embedded within the matrix (Graaff 2001). Bone tissue can be divided in two major groups, namely, compact (cortical) and spongy (trabecular) bone in an 80-20% ratio.

As the name implies, compact bone tissue is denser and with less open spaces then the spongy bone. Blood vessels penetrate the compact bone, orienting bone substance, osteocytes and lamellae. Bone-axis-oriented vessels are known as central (or haversian) canal and contain small nutrient vessels and nerves (Graaff 2001). These overall column-like systems formed by a central canal, contiguous lamellae and osteocytes, are designated as haversian systems, or osteons.

On the other hand, spongy bone tissue has more empty spaces and is composed of several bone plates named trabeculae, which are distributed along the in-bone tensile strengths lines. Although spongy bone is highly vascularized and provides great strength to bone with minimal weight, no blood vessel is able to penetrate trabecular plates, which are composed of osteocytes and have osteoblasts in their surface. Given this, these cells have to obtain nutrients through canaliculi structures.

In a layout's point of view, cortical (compact) bone is concentrated in the bone exterior whilst the trabecular (spongy) bone is in its interior, as can be seen in Figure 1.

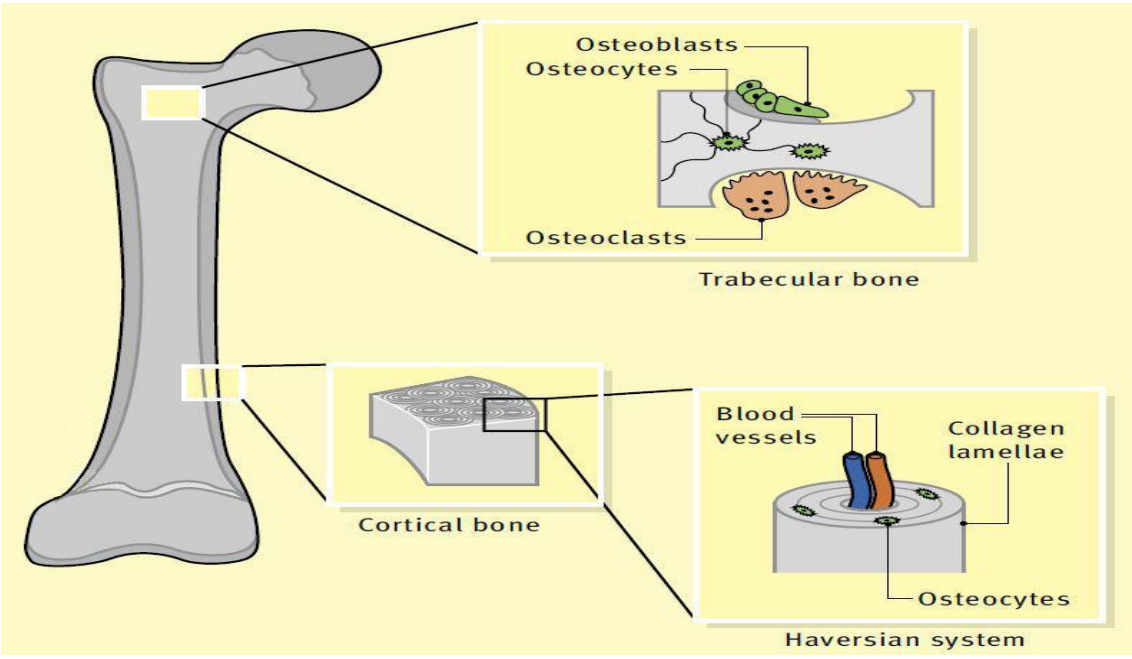

Figure 1- Bone Structure Layout, showing trabecular bone (interior region) and cortical bone (exterior region) as well as their respective components (Adapted from Ralston 2005).

The skeletal system includes long, short, flat and irregular bones and performs several functions such as support, protection, hematopoiesis and mineral storage (Graaff 2001). Its maintenance is based in a continuous dynamic process of bone remodeling which comprises bone tissue morphogenesis, growth, modeling and resorption (Lieberman & Friedlaender 2005).

1.1.2. Bone Tissue Cells

The bone's formation and maintenance processes are executed by different types of bone cells, for example, osteoblasts and osteoclasts are responsible for bone formation and degradation, respectively.

Osteoblasts are cuboidal shaped bone-forming cells that arise from pluripotent mesenchymal progenitor cells. They produce constituents of the extracellular matrix and are also very rich in alkaline phosphatase, which participates in the mineralization process (Dorozhkin 2007). Osteoblasts are displayed in rows in the inner layer of the periosteum and the endosteum (Stewart 2004). As mineralization takes place, osteoblasts become gradually jammed within the bone matrix, being eventually converted to osteocytes (Maniatopoulos et al. 1988; Sikavitsas et al. 2003)

Osteocytes are responsible for the maintenance of bone healthiness by regulating its metabolism and remodeling. Individual osteocytes connect with each-other, as well as with osteoblasts, and communicate via gap junctions, creating a highly interconnected network within the bone matrix (Hollinger et al. 2004). This intercommunication allows the detection of bone alterations and its communication to neighboring osteoblasts and osteoclasts. Osteocytes also assist in the nutrients transfer and waste products removal from bone (Stewart 2004).

As for osteoclasts, they derive from fused bone marrow stem cells and are responsible for the bone's resorption, through bone mineral dissolution and bone matrix digestion. The bone is resorpted in a specialized area of the osteoclastic cell membrane called the "ruffled border" (Dorozhkin 2007).

Besides osteoblasts, osteocytes and osteoclasts, there are other bone cells (osteogenic cells) that are recruited in case of trauma (e.g fracture); and bone-lining cells, that are involved in calcium and phosphate carriage along the bone matrix (Graaff 2001).

1.1.3. Extracellular matrix

Adult bone extracellular matrix (ECM) is composed of organic matrix (33%), containing type I collagen, minor collagens and non-collagenous proteins, lipids and complex carbohydrates (Wen et al. 2010). Osteoblasts are responsible for type I collagen production, which constitutes 65 to 90% of the organic matrix, as well as noncollagenous proteins such as osteopontin, osteonectin or osteocalcin. These bone-forming cells, are known to deposit about 0,5 μm of ECM per day (Tate 2008).

Type I collagen is responsible for the bone's elastic properties and acts as a support for bone mineral deposition, since the mineral crystals are aligned along the collagen fibers axis. In addition, bone also contains small amounts of type III, type V, and type XII collagen that trim the type I fibrils, and may affect the properties of the tissue (Hollinger et al. 2004).

Noncollagenous proteins represent only 5% of the dry bone matrix. However, they're of major importance since they're thought to control the organization, turnover, and mineralization of the bone matrix (Hollinger et al. 2004). Osteopontin is the major phosphorylated glycoprotein of bone. Its expression is usually increased when phosphate concentrations are increased, signifying that it is a mineralization key regulator. Osteonectin is another glycosylated phosphoprotein, commonly found in mineralized tissues. It binds to both type I and IV collagen and it has been described as a mineral deposition enhancer and a mineral crystal growth inhibitor, it also regulates metalloproteases' activity, that are in charge of extracellular matrix degradation (Hollinger et al. 2004). Osteocalcin is a regulator of bone mineral formation and growth and it can also regulate bone mineral remodeling, due to its interaction properties with bone mineral crystals (Hollinger et al. 2004).

Regarding bone's inorganic matrix (67%), it is composed primarily of calcium (Ca^{2+}) and phosphorus (PO_4^{3-}) mineral salts, that are usually deposited as hydroxyapatite crystals ($Ca_{10}(PO_4)_6(OH)_2$ (Hollinger et al. 2004).

The organic portion of the bone gives it flexibility, while the inorganic portion provides strength. Both features are closely related for the reason that if the bone is depleted from its inorganic components, particularly calcium phosphate, it becomes too flexible. Conversely if collagen reaches low concentrations the bone becomes very brittle, which results in bone structure weakening or shattering (Stewart 2004).

1.1.4. **Bone Morphogenesis**

Bone tissue formation begins at approximately week 4 of the embryonic development and is originated from the mesenchyme. Some of the embryonic mesenchymal cells are transformed into chondroblasts and develop a cartilage matrix which is then replaced by bone in a process known as endochondral ossification (Graaff 2001). Bone morphogenesis (or ossification) is a two-step osteoblast derived process in which the first stage involves osteoblast elongation and binding to other osteoblast while the second includes extracellular bone matrix formation (hydroxyapatite and collagen) around the cells, hereafter designated as osteocytes.

Two different patterns of ossification occur, the membranous and the endochondral ossification. Membranous ossification is based in the aggregation of osteoprogenitor cells, future osteoblast, which form a membrane of connective tissue and gradually creating thin bone trabeculae (Tate 2008). Later, this gives rise to cancellous bone. As cancellous bone is formed, bone surrounding cells generate the periostium allowing osteoblasts deposition between the previously formed cancellous bone and the periostium. Thus, membranous ossification creates a compact-cancellous-compact overall layout in the new bone structure.

Moreover, it allows the conversion of non-laminar to laminar bones and contributes to the bone's final form.

Endochondral ossification is the process by which most of the skeleton is formed and resides in the formation of a cartilage model which is then gradually replaced by bone. These cartilage models (formed through mesenchymal cells' condensation and by their differentiation into chondrocytes) are invaded from center to edges by a mixture of cells that establish the primary and secondary centers of ossification (Mackie et al. 2008). Primary centers of ossification appear in initial stages of fetal development whilst the secondary appear in the epiphyses at approximately one month before birth (Tate 2008). These centers of ossification gradually spread through the remaining cartilage, replacing it completely by the time skeletal maturity is reached (exception being made for the articular surfaces) (Mackie et al. 2008).

1.1.5. Bone Growth

Bone morphogenesis begets bone growth and it can occur as appositional or endochondral growth. The first consist in the formation of new bone on top of the old one. On the other hand endochondral growth is based in the same principle stated before for the endochondral ossification, that is to say, cartilage is formed and then progressively replaced by bone.

Appositional growth is responsible for long bones' widening (diameter increase) and has a major role in the growth of other bone types. Bone surface osteoblasts sequentially divide, creating new bone layers while bone interior osteoblasts secrete bone matrix and turn into osteocytes. This multiple layer increase allows an increase in the bone's width (Tate 2008).

Endochondroal growth usually implies an epiphyses proliferation which grows the diaphysis length. This process is due to a continuous cartilage formation and calcification which stacks chondrocyte layers, therefore increasing bone length (Tate 2008).

1.1.6. Bone Remodeling and Resorption

Bone remodeling is the name given to old bone tissue replacement by osteoclastic activity that is responsible for old bone tissue removal as osteoblasts creates new one. This process is usually required in cases like bone's tensile strength related adjustment or in the previously stated haversian systems formation. Osteoblastic activity is influenced by mechanical tensile strength, that is to say, it's increased when in high stress and diminished when in rest (Tate 2008). A schematic of the overall bone dynamics is displayed in Figure 2.

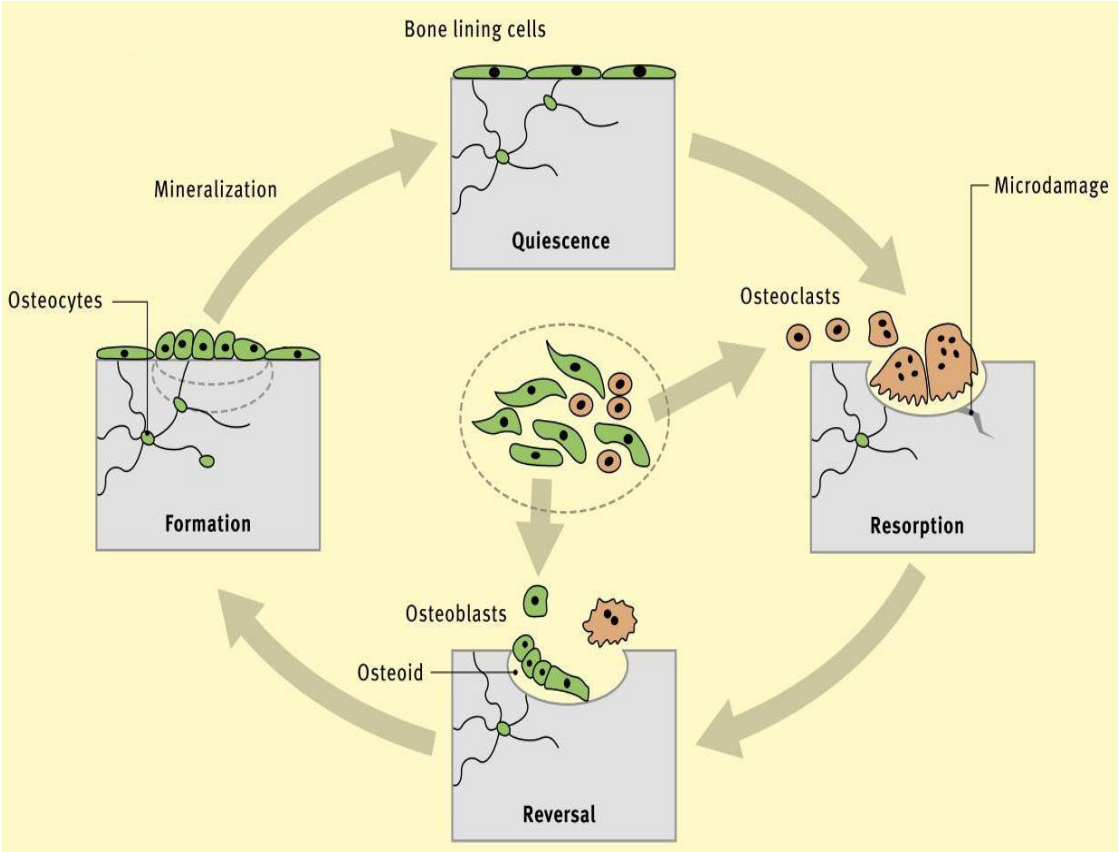

Figure 2- Bone dynamics' process, evidencing bone formation by the osteocytes followed by a mineralization step and the remodeling stage inherent to bone damage. Bone resorption by the osteoclasts is also represented (Adapted from Ralston 2005).

Regarding bone lesions, the most frequent type is fracture — the cracking or breaking of a bone. Fracture healing is a process involving an intricate series of biological events (Figure 3) and is usually classified according to type and severity of the lesion. Thus, they're generally divided in two major categories: primary and, the most common, secondary bone healing (Lieberman & Friedlaender 2005).

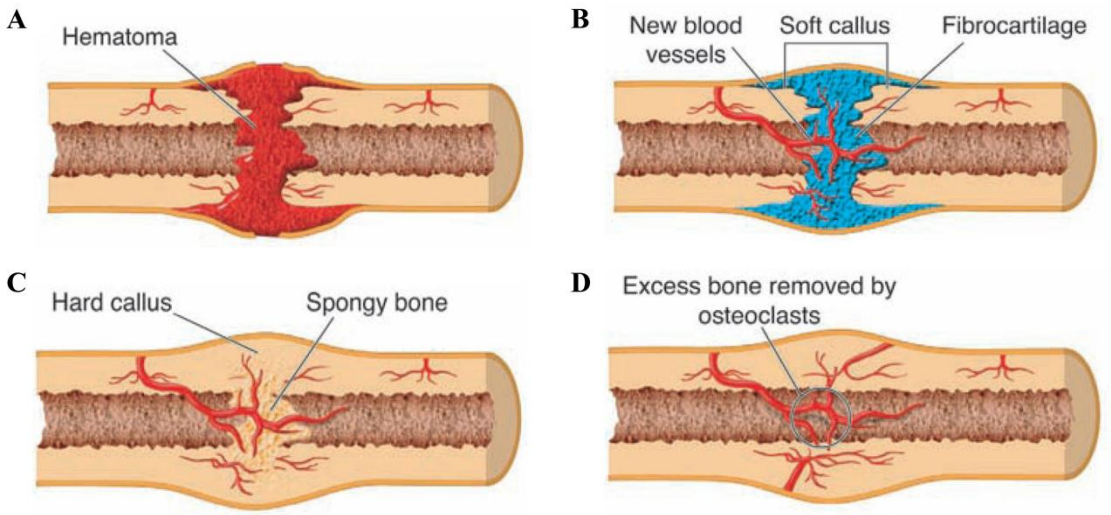

Figure 3- Stages of a bone fracture repair. A- Blood escapes from ruptured blood vessels and forms a hematoma. B- Spongy bone forms in regions close to developing blood vessels (Soft callus); fibrocartilage forms in more distant regions. C- Fibrocartilage and Soft callus are replaced by a Hard callus. D- Osteoclasts remove bone tissue excess, making new bone structure similar to the original (Adapted from Stewart 2004).

Primary bone healing can be considered clinically rare since most fractures are treated in a way that results in some motion allowance for the patient (e.g. cast immobilization). This healing method is able to achieve bone union without external callus formation. As for the most common secondary bone healing, it occurs when there is no rigid fixation of the fractured bone ends thus leading to the development of a fracture callus. This process is a little more complex and consists of an inflammatory phase, a reparative phase, and a remodeling phase (Lieberman & Friedlaender 2005).

1.1.7. Bone Diseases

Bone tissue can suffer from several bone incapacitating diseases, usually due to an imbalance between the bone's formation and breakdown processes i.e. imbalances in the normally coupled activity of osteoblasts and osteoclasts (Hollinger et al. 2004).

Diseases like osteoporosis are associated with a decrease in total bone density. Osteoporosis risk factors include aging, inactivity, poor diet, and hormonal imbalance. It is most common in older women due to low estrogens levels after menopause which leads to an increased bone resorption that is not properly complemented by new bone formation. Bone fractures, particularly at the pelvic girdle and vertebrae, are quite usual in osteoporosis patients, since bones become too brittle to support body weight (Graaff 2001).

Osteomalacia is defined as the loss of bone mineral and an increase in osteoid (Hollinger et al. 2004). This augments bone flexibility and consequently causes them to deform (Graaff 2001). The major cause for osteomalacia is vitamin D deficiency, probably resulting from lack of sunlight or a poor diet. This often leads to hypocalcaemia and hypophosphataemia (Whyte & Thakker 2009).

Paget's disease is characterized by an increase in osteoclastic bone resorption, accompanied by an augmented and disorganized bone formation. This usually leads to bone hypertrophy and structural defects causing pain and bone deformity. Causes for Pagetic bone lesions are not yet fully understood however changes in nutrition, mechanical loading of the skeleton, exposure to infections and ethnic differences are pointed as the major risk factors (Ralston 2008).

In order to overcome all these issues and limitations, Tissue Engineering has been studying bone regeneration techniques. Biodegradable implants, engineered to provide temporary support for bone fractures, or scaffolds that can serve as a substrate for seeded cells facilitating new tissue formation, are some of the tools that are discussed in the following section.

1.2. Tissue Engineering

1.2.1. Biomaterials

The concept of "biomaterial" is relatively recent. Yet, materials have been used along time aiming to solve health-related issues (Ratner et al. 2004).

The term biomaterial has alternately been used to describe materials derived from biological sources or to describe materials used for therapies in the human body. However, according to area experts, a biomaterial is “a compound, natural or synthetic, which is in interaction with biological systems" (Ratner et al. 2004).

Biocompatibility and biodegradability need to be considered, when entitling a material for a biomedical application. Biocompatibility can be defined as the ability of a material to perform a particular function in a specific organism or the ability to trigger an adequate response in the host. Biodegradability is the ability of a material to degrade within the body, without trigger any adverse response. A precise and accurate biodegradability may suppress a future need of surgery.

Identifying suitable biomaterials (either natural or synthetic) that promote cell adhesion, support cell growth, proliferation, differentiation and that properly degrade is the main step in the creation of TE scaffolds (Leong et al. 2008).

1.2.2. Biomaterials applications in Tissue Engineering

Tissue Engineering aims to create biological substitutes to repair or replace failing organs and tissues (Leong et al. 2008). Initially, materials used as implants were the same used in industrial applications. Pioneer surgeons designed their implants using materials usually applied in areas like chemistry, energy, mechanical and aerospace sciences (Navarro et al. 2008).

Materials like metals, polymers or ceramics aimed to be used as implants need to be carefully selected, since the human body is a highly corrosive environment. Given this, the first generation of biomaterials used for this purpose was as inert as possible, in order to reduce their corrosion and their release of ions and particles after implantation, but revealed good mechanical properties (especially in cases of bone replacement). The materials used for this purpose were, for example, titanium alloys or similar combined with ceramics like alumina.

Later, the concept of biocompatibility and biodegradability is assessed by a series of *in vitro* and *in vivo* standardized tests. Bioactive materials like the bioglass (45S5), developed by Hench in the 1970s, or calcium phosphate-coated titanium alloys were then classified as second generation materials.

More recently, materials are designed to be not only bioactive and biodegradable but also to stimulate specific cellular responses at a molecular level, depending on the damaged tissue that it is aimed to be repaired. These are considered the third generation materials.

These three generations should not be interpreted as chronological, but conceptual, since each generation represents an improvement on the requirements and properties of the biomaterials (Navarro et al. 2008).

For bone tissue regeneration, calcium phosphate based materials are commonly used in biomedical applications due to their good osteoconductive and osteoinductive properties (Perera et al. 2010). Since hydroxyapatite is the major mineral phase presented in the bone, it is usually the first selection in terms of material for bone regeneration scaffold fabrication (Perera et al. 2010).

A major feature in bone regeneration scaffolds is biodegradability. Preferably, the scaffold degradation profile should be designed so that it supports the construct until neotissue is formed. This being assumed, hydroxyapatite's low biodegradability levels become an issue when it is applied in scaffolds production for bone replacement. On the other hand, ß-Tricalcium phosphate has been *in vitro* tested and revealed better results both in bone formation and in the scaffold's degradation rate (Kondo et al. 2006).

Moreover, many biomaterials lack osteoinductive properties in the absence of additional osteoinductive agents, like bone morphogenetic proteins (BMPs). However, several reports have described osteogenesis by calcium phosphate alone, and such osteoinductivity is a desirable feature for a bone-substitute material (Kondo et al. 2006).

1.2.3. Computer Aided Tissue Engineering

CATE was created by merging Tissue Engineering science with computed three-dimensional modeling techniques (Leong et al. 2008). CATE is usually divided in three main branches, (1) computer aided anatomical modeling; (2) computer aided tissue classification; and (3) computer aided tissue implantation (Sun & Lal 2002). The present thesis work plan focus the first branch of CATE.

New 3D modeling techniques like computer aided design/computer aided manufacturing (CAD/CAM) can be applied for the fabrication of 3D scaffolds with custom made structures, depending on the purpose of its application. Structural properties are one of the main aspects to be taken into account when designing a scaffold, so doing it accurately is fundamental since it will influence parameters like, e.g., gas/nutrient diffusion or cell adhesion. Factors governing scaffold design are complex and include considerations of matrix architecture, pore size and morphology, mechanics versus porosity, surface properties and degradation products.

CAD modeling allows the control of almost all of the scaffold's properties since it's able to define not only its geometry but also its pore size and shape, being able to reduce experimental trials and consequently production time and cost (Lacroix et al. 2009).

Ideally, the design of a scaffold through CAD is combined with rapid prototyping techniques in order to produce accurate physical scaffolds.

1.2.4. Image Acquisition Techniques

Computer Tomography is an imaging technique based in a photon emission/absorption level ratio, meaning that matter's density will determine the abortion rate of the X or gamma ray (usually X-Ray) (Duliu 1999). Given this, CT image acquisition relies in a 360º X-Ray analysis of the test subject, like described in Figure 4B. Through rotation of the X-Ray tube, as well as the detectors, numerous 3D density based cross sections of the body itself are obtained (matrixes), which are later on converted into two-dimensional (2D) CT images (Duliu 1999), as seen in Figure 4A.

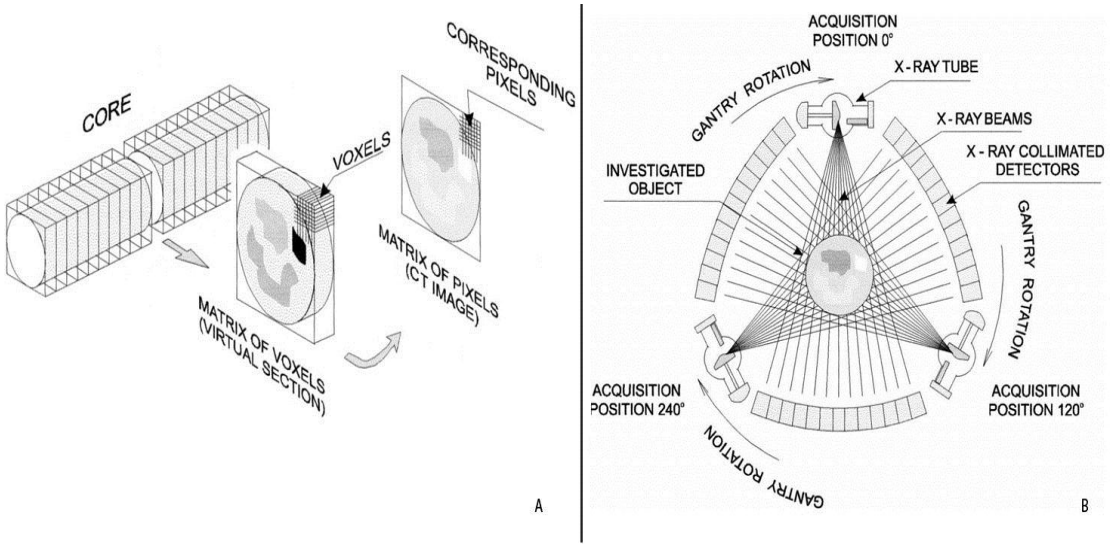

Figure 4- Computed Tomography basic concept and functioning principle. A- Schematic downsizing of the Core' cut sections to matrix of voxels and to a single unit of the matrix, known as Voxel (a Voxel in the virtual section directly corresponds to a pixel in a CT image). B- CT image acquisition procedure based in a 360º X-Ray analysis. (Adapted from Duliu 1999).

Medicine CT devices are often equipped with large performance intense ray tubes which are able to reduce running times to only a few seconds, depending on the test subject dimensions (Duliu 1999).

As for the Magnetic Resonance Imaging technique' foundation, it comprises the interaction between radiofrequency pulses, a strong magnetic field and a body tissue to obtain images of slices/planes from inside the body (Byrne 2008). The overall MRI process consists in the creation of a steady state of magnetism within the human body, by subjecting the body to a strong magnetic field, followed by its stimulation with radio waves, to change the protons' orientation. After this, the radio waves are stopped and the body's electromagnetic transmission is recorded, creating the body images (Byrne 2008). Data obtained by magnetic resonance is extremely detailed and can give accurate diagnostic information on various organs.

Since CT and MRI scans are non-invasive and non-destructive, they become excellent methodologies for different sciences like medicine or geology. However, these techniques provide slightly different information, one complementary with the other. CT is considered to

be the best system for 3D imaging of the bone structure, shape and geometry of defects since the 3D models are more readily generated from CT than from MRI scans (Krupa et al. 2007).

1.2.5. Computer aided anatomical modeling

Scaffold design using individualized patient data allows the production of accurate and specific models, capable of fitting perfectly into the patient's bone defect.

CT and MRI are diagnostic techniques that can provide such data for an accurate three-dimensional volume reconstruction (Sun & Lal 2002). Since these image acquisition techniques rely in the capture of 2D multiplanar images, the loss of the third dimension is an inherent problem. CAD software allows a three-dimensional reconstruction so that volumes and surface areas of the reconstructed objects may be determined (Krupa et al. 2007). Patient's specific CT and/or MRI data can be exported in standard Digital Imaging and Communications in Medicine (DICOM) format, and imported in CAD software, such as Lightwave, allowing volume render.

The main color of the DICOM image is black, which denotes null. During CT imaging, solid human tissues are represented as white. Therefore, a grey-level amplitude change occurs at the edge from black to white (C. Wang et al. 2010). Given this, by thresholding grey levels it is possible to differentiate different densities within the 3D model. This step allows skin, muscle and bone densities' parting.

Apart from CT-based 3D models' creation, other 3D models with different geometries may also be developed. 3D design software's, like Solidworks, can create nearly any desirable 3D geometry which can be used to produce the models' shape according to its future application (Duan & M. Wang 2010).

When either a CT-based or a 3D-designed model creation ceases, the files must be stored in stereolithography (STL) format for virtual reality simulation as well as for RP fabrication.

1.2.6. Rapid prototyping techniques for scaffold manufacturing

RP embraces a wide range of new technologies for producing accurate parts directly from CAD models in few hours, with little need for human intervention. RP techniques can be easily automated and integrated with imaging techniques to reconstruct 3D solid models that are customizable in size and shape for biomedical specific applications.

Available RP processes commonly used in prototyping anatomical models include, for example, Selective Laser Sintering (SLS) that employs a CO_2 laser to selectively sinter thin layers of powdered materials, forming solid 3D objects; Fused Deposition Modeling (FDM), builds parts by depositing a stream of hot viscous material onto a base plate or previously deposited material; Three-dimensional printing (3DP) (Figure 5), creates models by spraying liquid binder through ink-jet printer nozzles on to a layer of powder material. It is a layer-by-layer fabrication process in which successive 2D layers of the STL 3D model is printed. The

printer deposits layers of powder and binder, interchangeably. The model is completed upon removal of the unbounded powder. (Kruth et al. 1998; Lam et al. 2002; Yan 1996)

Figure 5- Photo of a Zcorporation Zprint 310 plus 3D-printer, used in this study.

Chapter II

Materials and Methods

2. Materials and Methods

2.1. Materials

The material used for the 3D printing of the scaffolds was a commercially available β – TCP powder, purchased from Panreac (Barcelona, Spain) with 90% of the particle diameter (d90) lower then 36,24 μm and a mean particle size of 11,64 μm, measured in a Beckman Coulter LS Variable Speed Fluid Module Plus (Brea, CA, USA). Human osteoblast cells (CRL-11372) were purchased from American Type Culture Collection (VA, USA). Amphotericin B, L-glutamine, Dulbecco's Modified Eagle Medium-F12 (DMEM-F12), ethanol (EtOH), glutaraldehyde, penicillin G, phosphate-buffered saline (PBS), ethylenediaminetetraacetic acid (EDTA), streptomycin and trypsin were purchased from Sigma (Sintra, Portugal). Fetal bovine serum (FBS) was purchased from Biochrom AG (Berlin, Germany). The 3-(4,5-dimethylthiazol-2-yl)-5-(3carboxymethoxyphenyl)-2-(4-sulfophenyl)-2H-tetrazolium, inner salt (MTS) was purchased from Promega. T-flasks and 96-well plates were purchased from Nunc (Denmark).

2.2. Methods

2.2.1. 3D Anatomic Modeling

Anonymous CT data from a patient's hand was obtained from Centro Hospitalar da Cova da Beira in standard DICOM format, and imported in CAD software – Lightwave (NewTek, San Antonio, TX, USA), in order to render a 3D volume. About 700 slices were reassembled and slice matrices, dimension of 512x512, were obtained with a pixel (voxel) size of 219x219x300 voxels. This data was used to create the hand model (Figure 6).

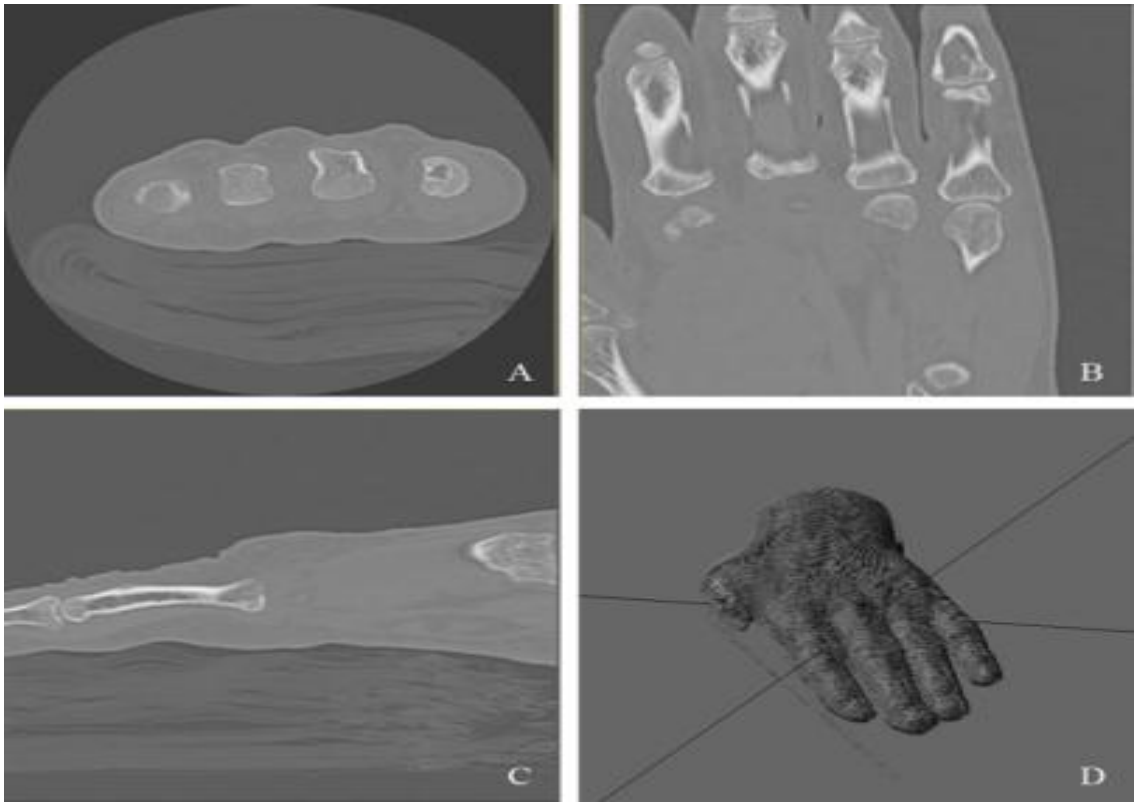

Figure 6 - Multiplanar 2D Images aquired from a CT scan and a 3D Hand Volume. A- Image acquired from the Y-axis; B- Image acquired from the Z-axis; C- Image acquired from the X-axis; D- Patient's hand 3D volume.

Due to tissue density differences, and by applying black and white gradients in the Lightwave software, it was possible to distinguish skin, muscle and bone in the CT image. This step allowed the creation of an accurate skeleton hand model.

The 3D geometrical vector based model, also known as polygon triangular mesh (which is the equivalent to the mathematical boundary of the volume/tissue) was created with Lightwave software allowing the edges of the model to be defined.

Since the mesh created with Lightwave software was very irregular and sharp edged, it was necessary to export it into another 3D modeling program, called MeshLab (Open Source Program). The use of this software allowed the obtention of a more accurate and clean version of the bone tissue volume. The left hand's ring finger proximal phalange was isolated in order to facilitate the scaffold's fabrication by the 3D printing process.

Simultaneously, solid cylinder ß-TCP scaffold, with a diameter and length of 10mm and 20mm respectively, were designed in Solidworks 2010 (Concord, MA, USA) and produced with the purpose of studying the influence of the sintering temperature on the mechanical strength, phase stability and also to evaluate possible limitations in the fabrication process.

2.2.2. Production of ß-TCP scaffolds

The 3D models were printed in a ZCorporation 3D-Printer (Portsmouth, NH, USA) Zprinter 310 Plus model. The 3D-printing process is based in a layer-by-layer construction in which powder and binder layers are alternately built on the construction tray.

The different 3D models were distributed along the virtual tray using the machine's standard software (Figure 7). This software allowed the operator to configure all the printing parameters like the powder type, shell and core binder's concentration (250%/250%) as well as the layer thickness. In the present work the layer thickness was defined as 0,0875mm, by doing so the ß-TCP particle size was comprised in the machine's resolution since, as stated before, d90 ≤ 36,24 µm.

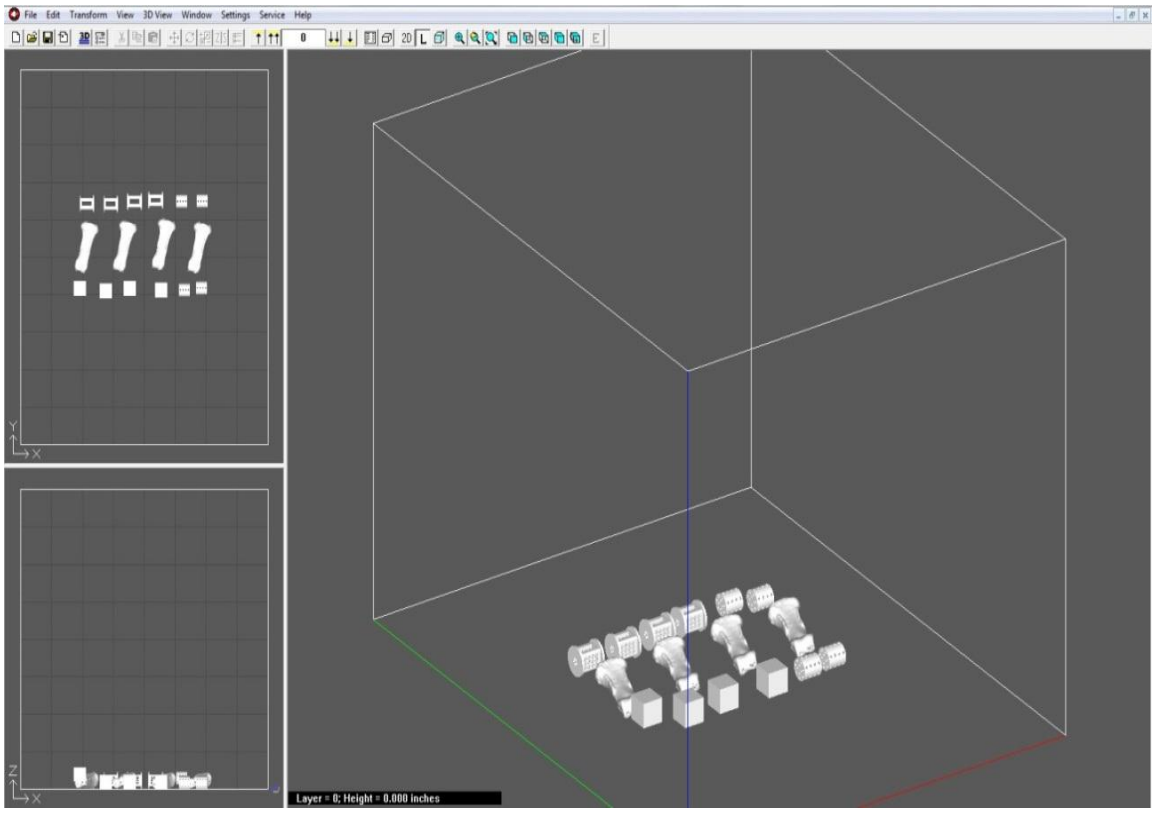

Figure 7- Printer's software featuring the 3D models displayed along the virtual tray. The virtual model's layout in the software will directly correspond to the position of the real model in the Printer's building tray. Multiple model designs were performed.

After the printer's setup was completed, the ß-TCP powder and the printer's standard zb60 binder were loaded into the respective feeding trays and the printing process was started.

As previously stated, different scaffold models were printed in order to perform mechanical and in vitro assays. The models included a real scale proximal phalange, cylindrical solid scaffolds (used in the mechanical test), and two porous cylindrical scaffolds with different geometries. After the printing process end, the samples rested for one hour in a warm environment (~38°C) inside the printer. Such procedure is required for these models

to stabilize. Then, the building tray was removed from the printer and the scaffold models were recovered. The excess of ß-TCP powder in the scaffolds was mechanically cleaned in a recycle station, so that the remaining powder could be re-used for future printings.

The mechanical strength of the scaffold is a key feature to be taken into account, since this property is fundamental for the application of this 3D construct in bone tissue regeneration. In the present work, green bodies (name applied to the non-sintered models) were very brittle, and consequently it was fundamental to increase their mechanical strength and resistance through a sintering process.

The sintering temperatures were carefully selected through the analysis of the ß-TCP's phase diagram (Figure 8) in order to avoid temperatures that are responsible for micro-fissures in ß-TCP aggregates. Then, the scaffolds were divided in four different test groups sintered at 1250°C, 1300°C, 1350°C and 1400°C. The sintering process was performed in a Thermolab 1400°C Muffle (Águeda, Portugal) with a temperature increase of 3°C/min, allowing not only the binder's removal from the scaffolds (at approximately 150°C) but also particle growth and crystalline structure stabilization.

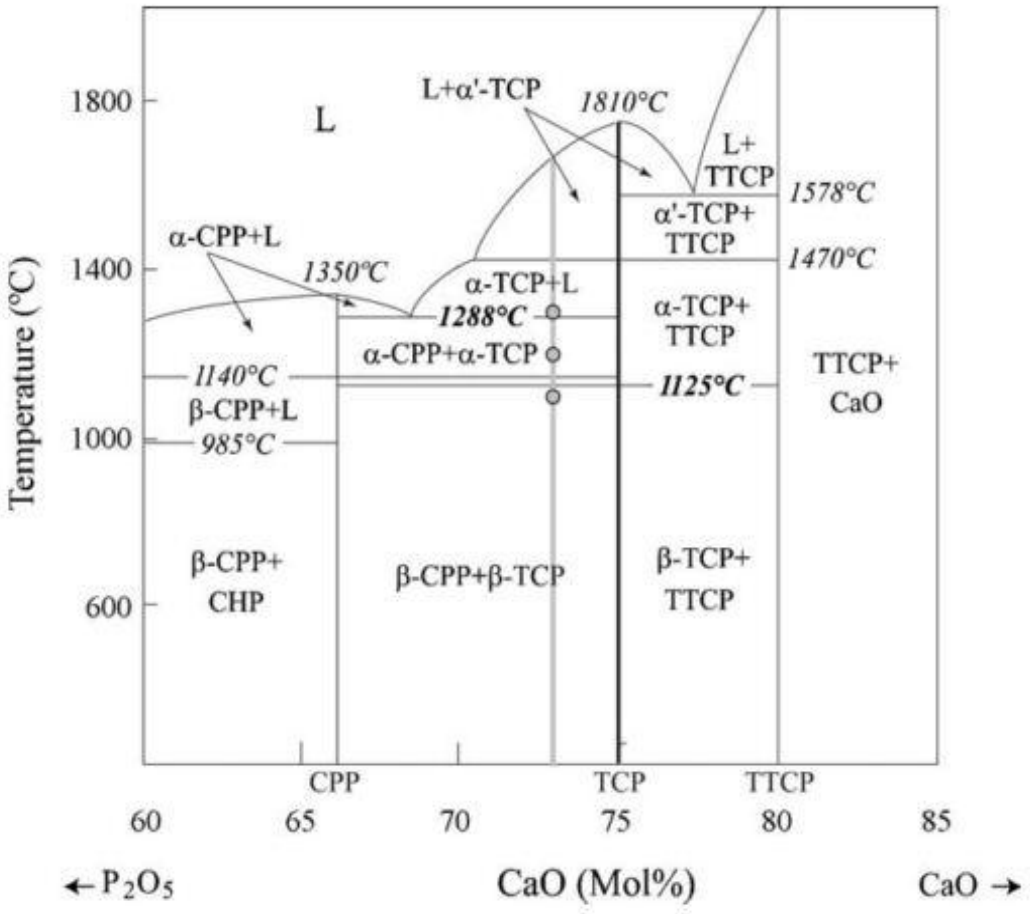

Figure 8- Tricalcium phosphate phase diagram used to select the ß-TCP model's ideal sintering temperature (Adapted from Perera et al. 2010).

2.2.3. Mechanical analysis of the β-TCP scaffolds

After the sintering process, scaffolds were submitted to a series of mechanical assays in order to compare their properties with those presented by the bone itself. The scaffolds' properties measured in these assays included dry weight, wet weight, 24 hour saturated weight, porosity, water absorption, bulk density, stiffness, shrinkage and compression strength.

For dry, wet and saturated weight determination, all samples were weighted in an Oertling VA204 (London, UK) model analytical balance. All the parameters were mathematical calculated according to *C20 ASTM Standards Test Methods*, exception being made for the compression strength which was determined by the *Brazilian test* (Proveti & Michot 2006).

Since the bone is a load-bearing structure, stiffness and compression strength are key features to a bone replacement substitute. Given this, the sintered cylindrical scaffold models were placed in a Zwick 1435 Materialprufung (Ulm, Germany) testing machine for compression strength determination, in which the samples were uniaxially compressed until maximum load was achieved. At least four specimens of each sintering temperature were tested.

2.2.4. Human osteoblast cell culture and proliferation assessment in the presence of sintered β-TCP scaffolds

Experiments involving cell culture were performed with human osteoblast cell line which was seeded with DMEM-F12, supplemented with heat-inactivated FBS (10% v/v), penicillin G (100 units/mL), streptomycin (100 µg/mL) and amphotericin B (0,25 µg/mL), in 75 cm^3 T-flasks. Detachment of confluent cells was achieved by a 5 min incubation in 0,18% trypsin (1:250) and 5mM EDTA. In order to stop trypsinization, an equal volume of culture medium was added to the free cells. A centrifugation step was performed and cells were resuspended with culture medium and seeded in new 75cm^3 T-flasks (Ribeiro et al. 2009).

To characterize sintered β-TCP scaffolds' influence in cell adhesion and proliferation, human osteoblast cells were seeded alongside the scaffolds in 96-well plates at a density of $15x10^3$ cells/well. Cell growth was monitored after 24 hours, using an Olympus CX41 inverted light microscope (Tokyo, Japan) equipped with an Olympus SP-500 UZ digital camera.

2.2.5. Characterization of the cytotoxic profile of the β-TCP

Sintered β-TCP scaffolds were distributed along a 96-well plate (Nunc, Roskilde, Denmark) and ultra-violet (UV) irradiated for 30 minutes, previously to cell seeding.

Human osteoblast cells were seeded in the 96-well plate (15×10^3 cells/well) and after 24 hours of cell-scaffold incubation, cell viability was assessed with an MTS Cell Proliferation Kit. To each sample 20 µL MTS were added, followed by incubation for 4 hours at 37°C, in a 5% CO_2 atmosphere. Absorbance at 492 nm was then measured using a Biorad Microplate Reader Benchmark (Tokyo, Japan). Wells containing cells in the culture medium without

biomaterials were used as negative control and ethanol was added to wells containing cells in the positive control.

Statistical analysis of cell viability results was performed using one-way analysis of variance (ANOVA) with the Dunnet's post hoc test. A value of *p<0,05 was considered statistically significant. Results of cells in the presence of different scaffolds were compared with negative and positive controls.

2.2.6. Scanning Electron Microscopy analysis

To further assess scaffold's morphology as well as cell adhesion, human osteoblast cells were grown in a 96-well culture plate, in which the multiple scaffolds were later added. After 3 days of culture, the samples were fixed overnight with 2,5% glutaraldehyde in PBS at 4°C. Then, samples were rinsed three times with PBS buffer for 2 min and dehydrated in graded ethanol of 70, 80, 90, and 100% during 5 min each. Subsequently, scaffolds were mounted on an aluminium board using a double-side adhesive tape and sputter coated with gold using an Emitech K550 sputter coater (London, UK). The scanning electron microscopy (SEM) images were obtained with a scanning electron microscope Hitachi S-2700 (Tokyo, Japan) with an acceleration voltage of 20kV at different magnifications.

2.2.7. Fourier transform infrared spectroscopy analysis

Fourier transform infrared spectroscopy (FTIR) was used to characterize the effects of different sintering temperatures in the ß-TCP structure. Absorbance infrared spectra from the sintered calcium phosphate samples and the raw powder (used as reference) were recorded on a Fourier transform infrared spectrophotometer Nicolet is20 (64 scans, at a range of 4000 to 400cm^{-1}) from Thermo Scientific (Waltham, MA, USA) equipped with a Smart iTR auxiliary module.

2.2.8. X-Ray diffraction analysis

X-Ray diffraction (XRD) analysis was performed in order to analyze the effects of the sintering process in the physical structure of the ß-TCP. Tests were carried on with the raw ß-TCP powder and with sintered samples (from all temperatures). Samples were scanned from 5° to 90° 2Θ with continuous scans at a rate of 1° 2 Θ min^{-1}, using a Rigaku Geigger Flex D-max III/c diffractometer (Rigaku Americas Corporation, USA) with a copper ray tube operated at 30kV and 20mA. The samples were mounted in silica supports using a double sided adhesive tape and then analyzed.

Chapter III

Results and Discussion

3. Results and Discussion

3.1. 3D-Modeling achievements

In the modeling process used in the present work, tissue density differentiation was obtained by applying black and white gradients in the Lightwave software. Skin and bone density levels are shown in Figure 9A and 9B, respectively. This differentiation allowed the obtention of a 3D skeleton model of the hand, a feature required since the scaffolds were aimed to be used for the production of a bone replica. However, the mesh obtained with Lightwave was of low resolution and so an improvement in the mesh surface quality was necessary. Such was achieved using MeshLab, and the evidence of the surface's quality enhancement can be seen in Figure 9C-D. The overall process of surface quality enhancement was performed in order to obtain a more accurate and precise virtual model that, in theory, would give rise to real models with higher quality.

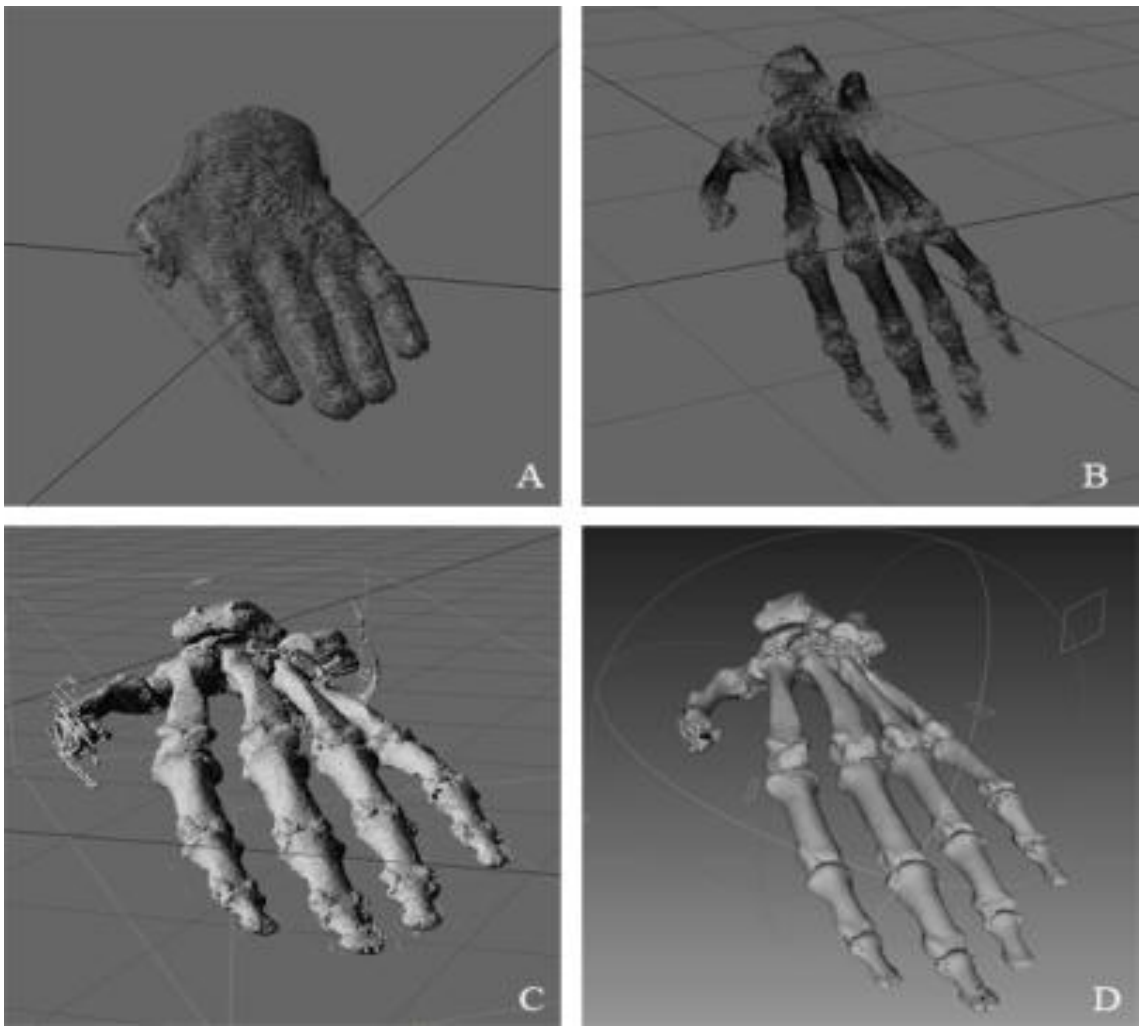

Figure 9- Skin and Bone Tissue density differentiation obtained through black and white gradients, with Lightwave. Skin density level (A); Bone density level (B); Triangular Mesh of the bone density volume (C); Mesh of the bone density volume improved in MeshLab.

As previously described, the left hand's ring finger proximal phalange was isolated from the hand model aiming to simplify the process of design, fabrication and sintering. Both the virtual and the real model are presented in Figure 10.

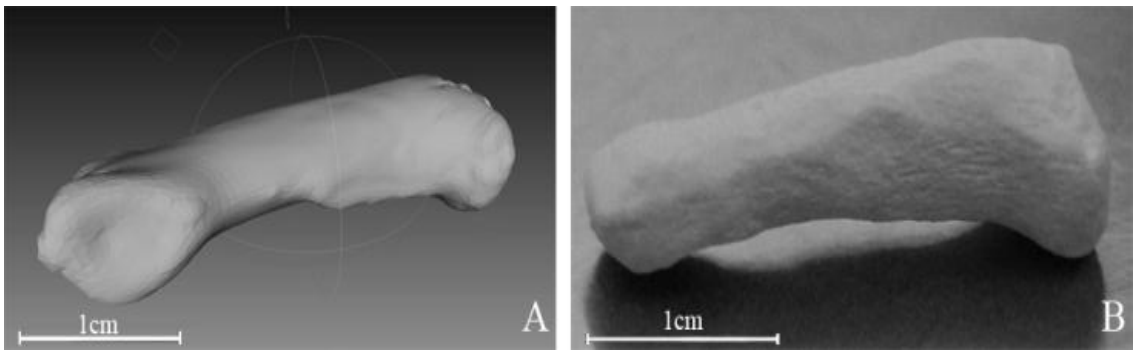

Figure 10- Images of the virtual left hand's ring finger proximal phalange phalange (a) and the printed model (b)

As stated before, Solidwork's designed scaffolds were also produced with the purpose of using them in mechanical trials. A comparison between Solidwork's virtually designed and printed models is shown in Figure 11.

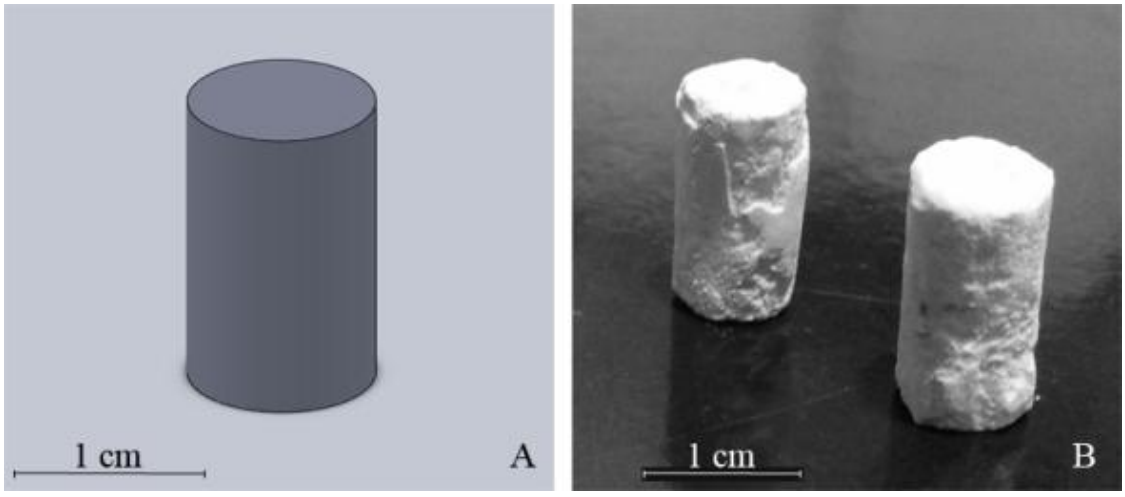

Figure 11- Image of a Solidwork's virtual model (A) and a printed model (B).

3.2. Mechanical characterization of the ß-TCP scaffolds

The macroscopic analysis of the scaffolds produced revealed that all structures are compact and presented a white color with a little rough and irregular surface.

In the present work, a mechanical characterization was performed as previously described in Chapter II. The results obtained revealed that, although there was a slight decrease in the apparent porosity and water absorption while the sintering temperature increased, the ß-TCP scaffolds' values for apparent porosity ranged between 46,07%–54,44%, which are similar to those previously published by other researchers (Ribeiro et al. 2011;

Ramay & Zhang 2004). This decrease in porosity may be related with an increase of bulk density (0,65g/cm^3 to 0,84g/cm^3), possibly due to the fact that porosity and density are inversely related or, on the other hand, that the processing of powder materials gave rise to structures with an inherent microporosity as a result of the voids formed between the powder particles (Ribeiro et al. 2011). An increase of bulk density without too much loss of microporosity is a good improvement bearing in mind the biomedical application proposed for the scaffolds herein produced.

Despite the improvements achieved, the sintering process caused a phenomenon known as shrinkage i.e. pre-sintered scaffolds were fabricated with a 10mm diameter and a length of 20mm. Although, a post-sintering measurement revealed a size decrease of about 30% in the same scaffolds, which is in agreement with the results previously described in the literature (Ribeiro et al. 2011; Seitz et al. 2009). Although shrinkage is also known to occur in the printing process (Seitz et al. 2009), due to powder granules coalescence, in the present study such was only observed after the sintering process.

Regarding the compression tests performed, an increase in the applied uniaxial force was notorious when higher sintering temperature scaffolds were used. The results here presented (ranging from 2,36 MPa to 8,66 Mpa) revealed that all the scaffolds' compressive strengths are in the range of the reported values for the trabecular bones (1-7 MPa) (Cordell et al. 2009), and that some of them (1350ºC and 1400ºC) even surpass this range of strengths.

The results of the mechanical assays performed on the ß-TCP scaffolds are presented in Table 1.

Table 1- Mechanical results obtained for the different tested parameters for all the sintered scaffolds.

	Apparent Porosity (%)	Water Absorption (%)	Bulk Density (g/cm^3)	Compressive Strength (MPa)
Scaffold 1250ºC	54,44±2,03	84,07±8,4	0,65±0,04	2,36±0,05
Scaffold 1300ºC	53,19±1,19	77,73±2,77	0,68±0,01	5,75±0,05
Scaffold 1350ºC	50,85±2,26	71,78±7,58	0,71±0,04	8,30±0,14
Scaffold 1400ºC	46,07±8,52	57,31±2,36	0,84±0,14	8,66±0,11

The ß-TCP's FTIR spectra obtained (Figure 12), for the powder and the sintered samples were analyzed and revealed a major band at 1020 cm^{-1} which is typically assigned to the components of the triply degenerated v3 antisymmetric P-O stretching mode, revealing inorganic phosphates components (Slósarczyk et al. 1997). Peripheral bands, at 962 cm^{-1}, were also obtained in all the analyzed samples and were assigned to v1, the non-degenerate P-O symmetric stretching mode (Slósarczyk et al. 1997). No relevant variations were observed between the different FTIR spectra.

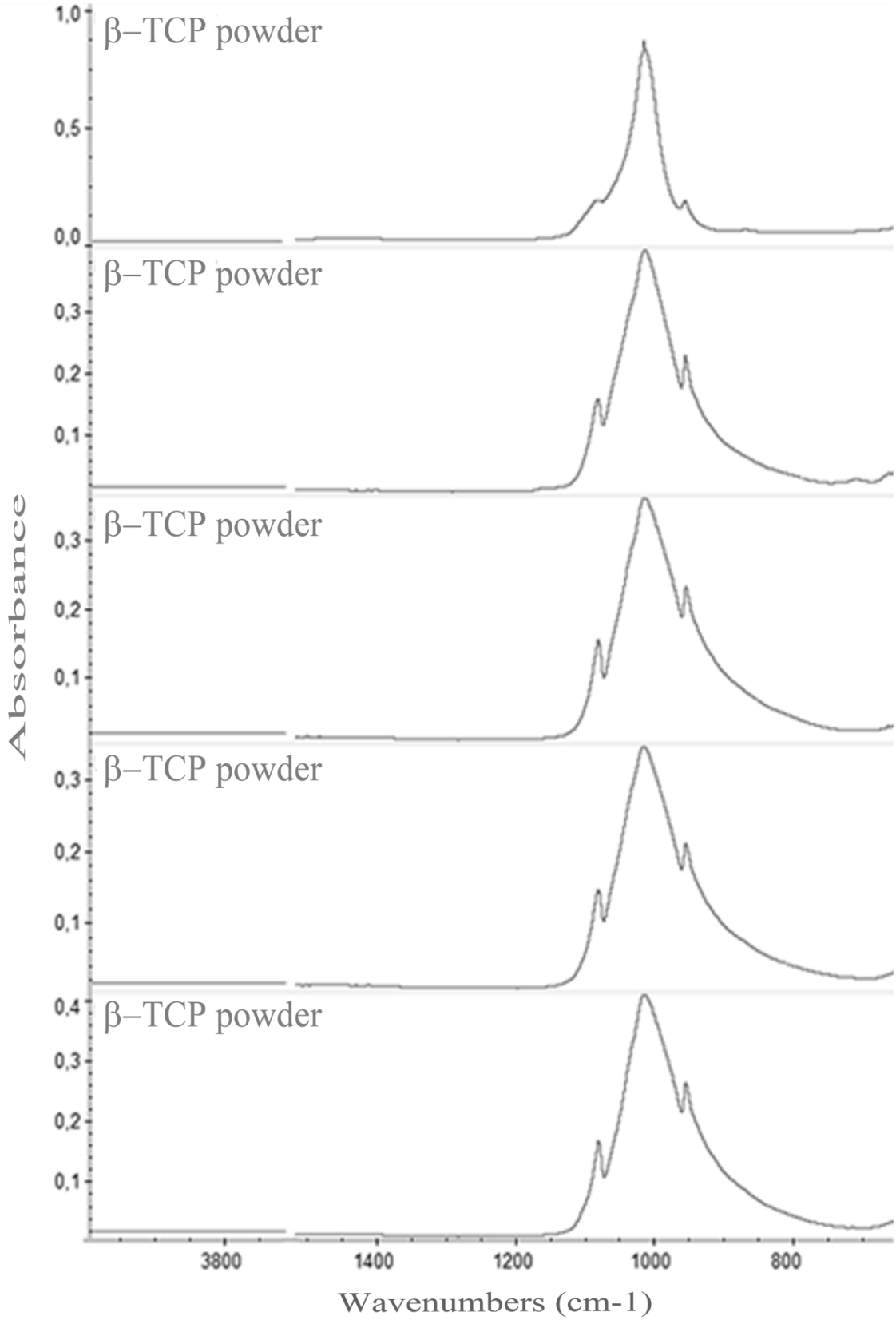

Figure 12- FTIR spectra obtained for the B-TCP powder (A) and for the ß-TCP models sintered at 1250°C (B), 1300°C (C), 1350°C (D) and 1400°C (E).

The XRD patterns are presented in Figure 13 and suggest that the sintering process induces crystallinity enhancement although no phase alteration was noticed. The comparison reveals that the peaks from the sintered samples match with those of the non-sintered sample. The spectra from sintered samples show better peak resolution.

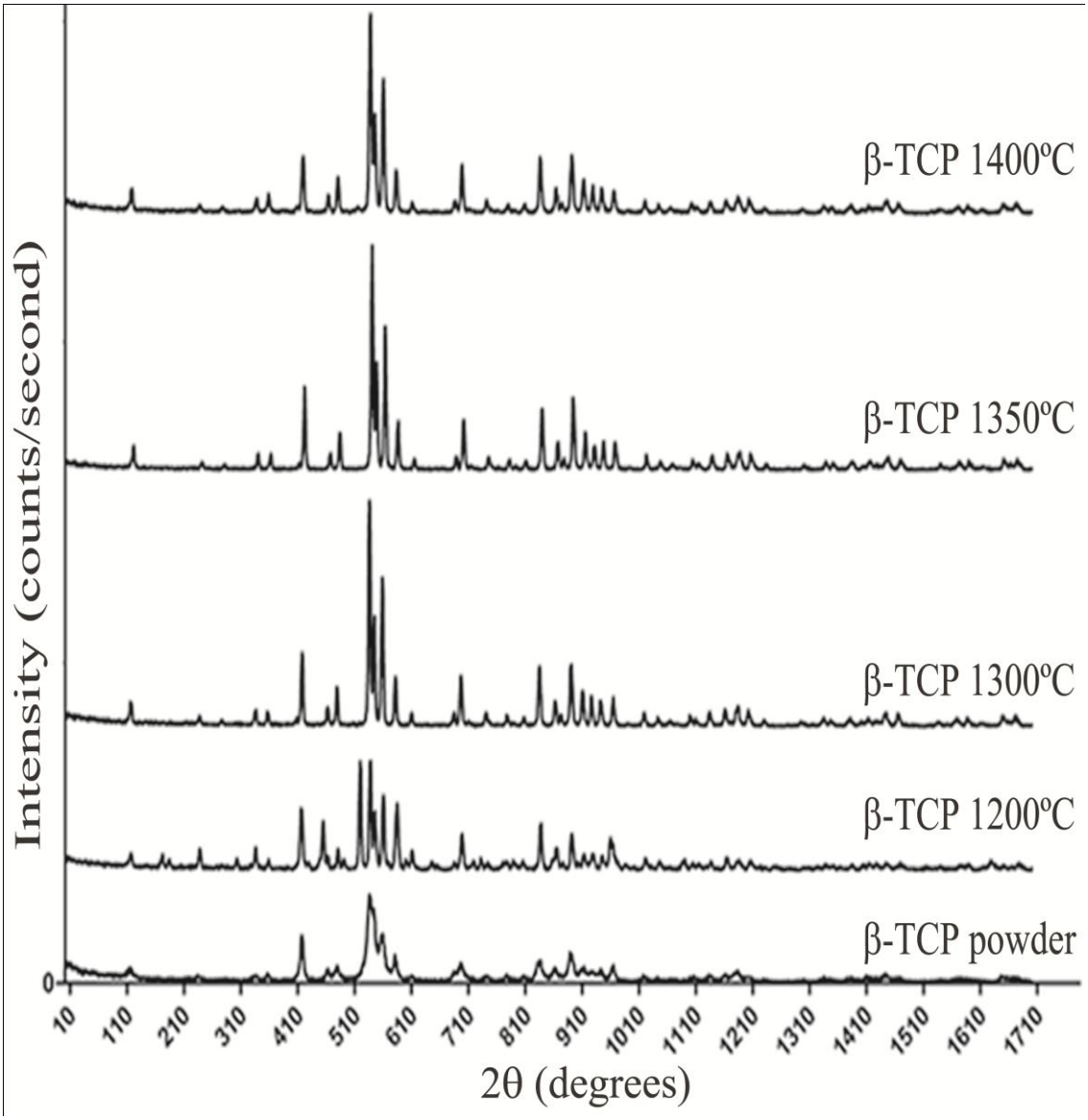

Figure 13- XRD profile of the B-TCP powder and of the ß -TCP models sintered at 1250°C, 1300°C, 1350°C and 1400°C.

Taking together both the XRD and FTIR results, we can conclude that the overall composition of the ß-TCP was not modified by the sintering process, when comparing the sintered models' features with the non-sintered powder. Nevertheless an enhancement in the crystallinity of the sintered scaffolds is notorious, evidencing a correlation of this property with the sintering step.

3.3. Characterization of ß-TCP's biocompatibility

In order to study the applicability of the ß-TCP scaffolds as biomedical devices, their cytocompatibility was studied through in vitro studies. Optical microscopy (OM) images were acquired after 24 hours and showed cell adhesion and proliferation in the vicinity of the ß-TCP scaffolds (Figure 14A-D) as well as in the negative control (Figure 14E). Regarding the positive control, no cell adhesion or proliferation was observed. Dead cells with their typical spherical shape can be observed in Figure 14F.

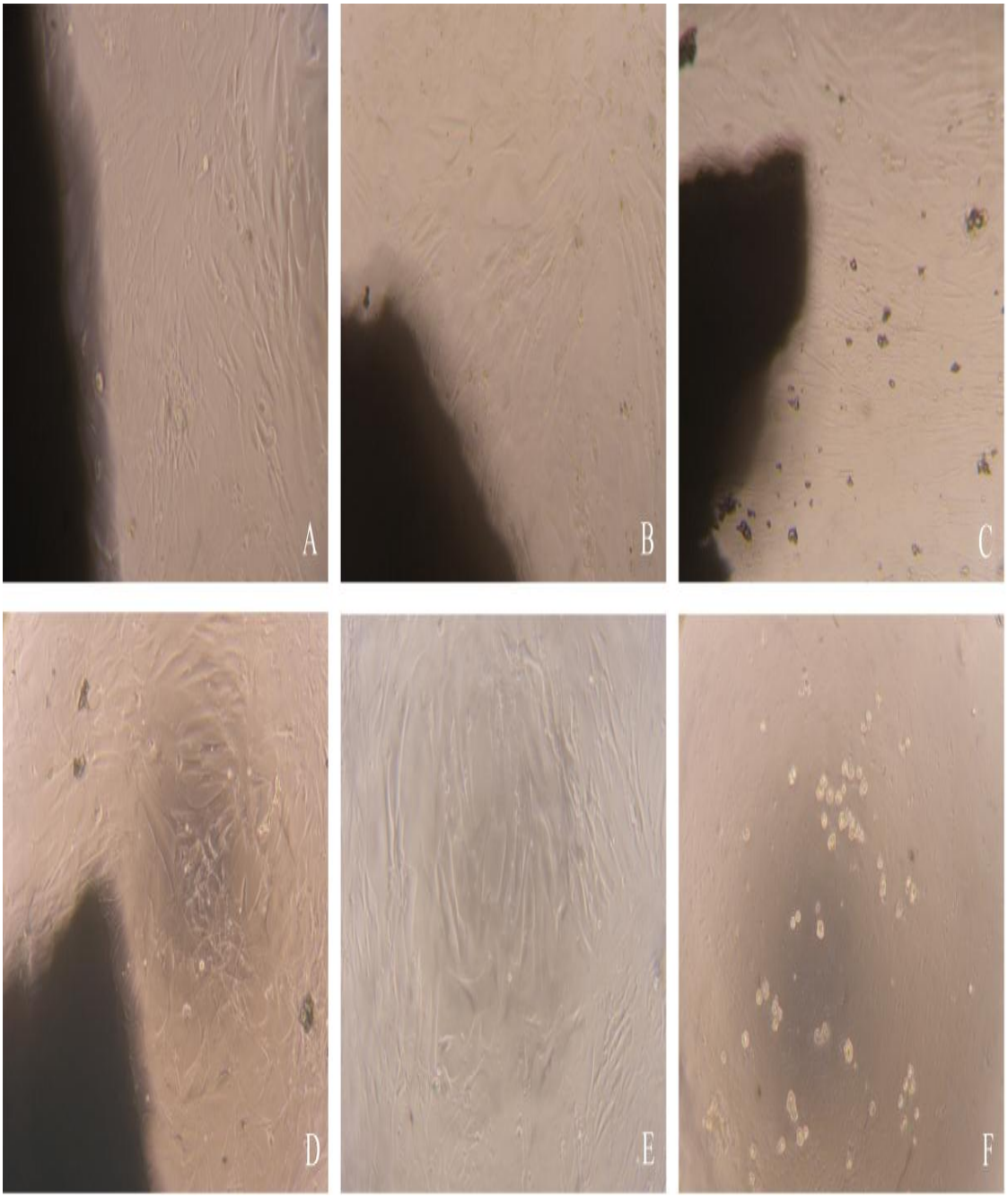

Figure 14- Optical microscopy photographs of human osteoblasts cells after being seeded in the presence of ß-TCP scaffolds sintered at 1250°C (A), 1300°C (B), 1350°C (C) and 1400°C (D). The negative and positive controls are presented in (E) and (F), respectively. Original magnifications 100X.

SEM images allowed the visualization of cells attached to all the ß-TCP scaffolds, after 3 days (Figure 15). Furthermore, SEM images revealed that scaffolds had a high level of microporosity and roughness, which is vital for osteoblasts to grow and proliferate as well as for nutrients and gas transport.

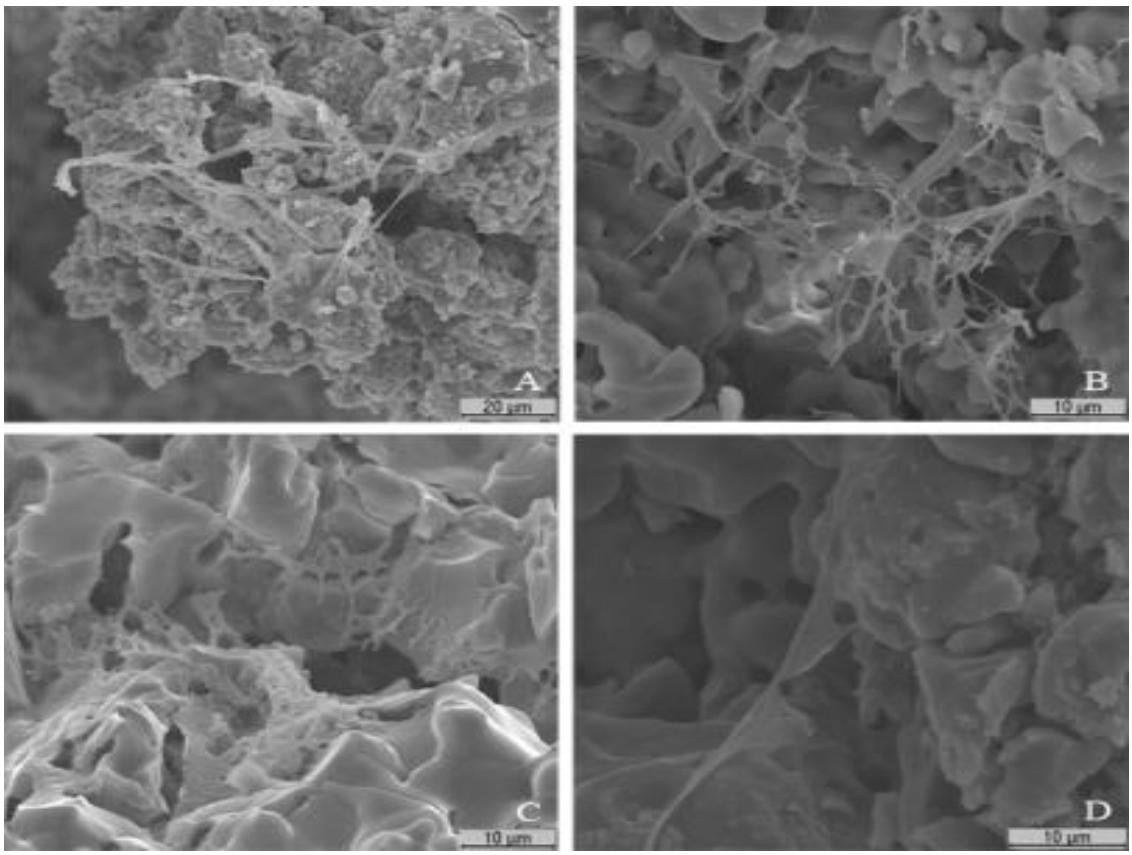

Figure 15- SEM Images of 1250°C (A), 1300°C (B), 1350°C (C) and 1400°C (D) sintered ß -TCP scaffolds with cells on the surface. Images had different magnifications: 1000x (A) and 2000x (B and C) and 2500x (D).

Moreover, the *in vitro* cytotoxicity was also evaluated by an MTS assay. The results (Figure 16) proved that cells in contact with the ß-TCP scaffolds showed higher cell viability than the positive control but lower than that of the negative control. As predicted, the positive control (K_+) showed no viable cells. The MTS assay showed a significant difference between positive control (*$p < 0,05$), the negative control and cells exposed to the different scaffolds after 24 hours, suggesting that the scaffolds did not affect cell viability.

Thus, the results obtained in OM, SEM and MTS suggest that the ß-TCP scaffolds have no acute cytotoxicity effect and that cells adhere and proliferate in the scaffolds' surface and vicinity.

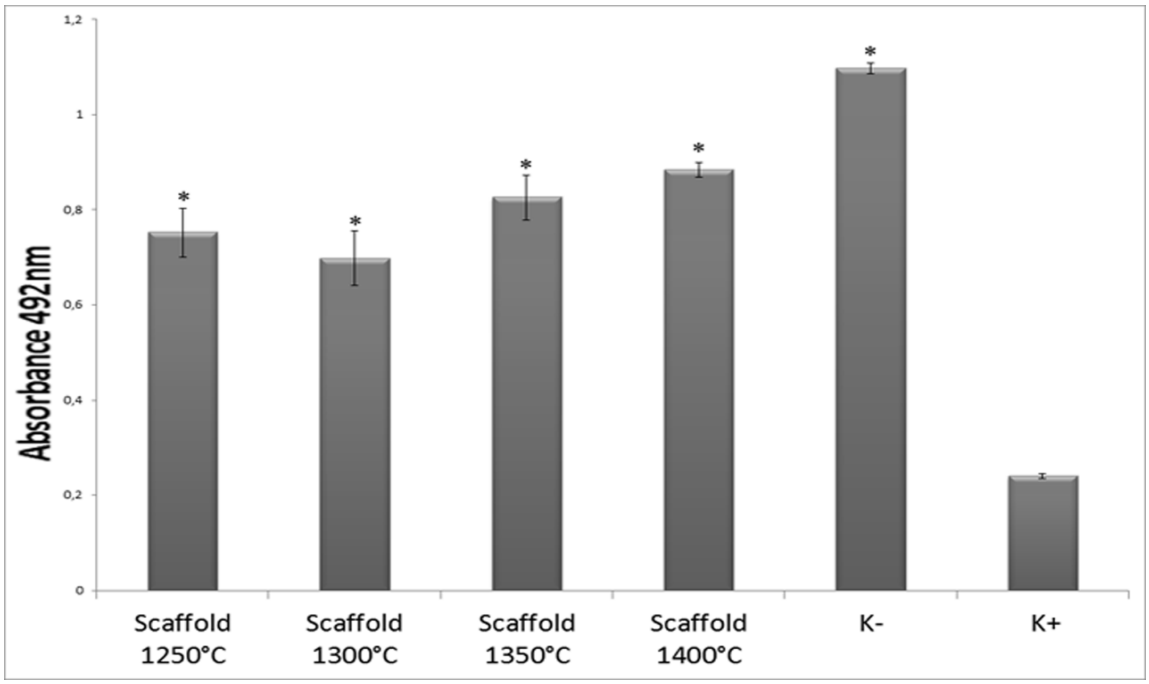

Figure 16- Evaluation of the cellular activity, after 24h, by the MTS assay. Negative control (K-); Positive control (K+). Each result is the mean±standard error of at least four independent experiments. Statistical analysis was performed using one-way ANOVA with Dunnett's posthoc test (*$p<0,05$).

Chapter IV

Conclusions and future perspectives

4. Conclusions and future perspectives

Bone degenerative and inflammatory problems affect millions of people worldwide. The solution to this often requires surgery and the incorporation of permanent, temporary or biodegradable devices. Therefore, orthopedic biomaterials are designed to perform certain biological functions by substituting or repairing different tissues such as bone.

In the present research work, the merging of computed tomography based 3D anatomic modeling and rapid prototyping techniques, in this case 3D printing, provided a fast, economical, individualized and specific scaffold fabrication process. Since the procedure described in this work is based in patient's specific data, it can be used to produce any required scaffold shape, with the possibility of recreating an entire patient's bone structure based on daily routine exams performed in health care institutions, representing therefore a major achievement.

In this study, different shaped ß-TCP scaffolds were fabricated and sintered at different temperatures in order to enhance their mechanical properties. The produced scaffolds, although they were in the trabecular bone's compressive strength range, lacked resistance for their application as cortical bone replacers. Given this, the porosity, bulk density and compression strength may be further improved by controlling parameters such as particle size distribution, sintering temperatures/ sintering time length or the binder's concentration. The SEM images and the *in vitro* cytotoxic assays performed showed a relatively good cell-scaffold interaction, thus revealing the scaffolds' biocompatibility. The scaffolds will be further evaluated through *in vivo* studies.

Moreover, scaffolds' coating with growth factors (GF), like BMPs, or Arginine-Glycine-Aspartic acid (RGD) sequences, that enhance cell attachment, will aim to improve it as a bone substitute. However, this immobilization needs to be performed after the sintering process since any proteins previously bind to the scaffolds' surface or in its core will be denatured, due to the high temperatures. Methodologies like electrospinning or surface modification, for example chemisorption, may overcome the issue stated in the last paragraph considering that the proteins/GF are added after the sintering process. Additionally, procedures involving the incorporation, in the scaffold loaded with GF, of previously-grafted stem cells from the patient may induce cell differentiation in the specific target tissue and so enhancing its regeneration.

Based on the results herein obtained it can be stated that the exploitation of individualized scaffold design combined with rapid prototyping may lead to successful development and translation of not only these tested ß-TCP bone-like scaffolds but also other types of scaffolds for biomedical load-bearing applications.

Bibliography

Bibliography

Byrne, A., 2008. Paediatric MRI. *Current Anaesthesia & Critical Care*, 19(5-6), pp.315-318.

Cordell, J.M., Vogl, M.L. & Wagoner Johnson, A.J., 2009. The influence of micropore size on the mechanical properties of bulk hydroxyapatite and hydroxyapatite scaffolds. *Journal of the mechanical behavior of biomedical materials*, 2(5), pp.560-570.

Dorozhkin, S.V., 2007. Calcium orthophosphates. *Journal of Materials Science*, 42(4), pp.1061-1095.

Duan, B. & Wang, M., 2010. Customized Ca-P/PHBV nanocomposite scaffolds for bone tissue engineering: design, fabrication, surface modification and sustained release of growth factor. *Journal of the Royal Society, Interface / the Royal Society*, 7(5), pp.615-629.

Duliu, O., 1999. Computer axial tomography in geosciences: an overview. *Earth-Science Reviews*, 48(4), pp.265-281.

Graaff, K.M.V.D., 2001. *Human Anatomy* 6th ed., Mcgraw.

Hollinger, J.O. et al., 2004. *Bone Tissue Engineering* 1st ed., CRC Press.

Kondo, N. et al., 2006. Osteoinduction with highly purified beta-tricalcium phosphate in dog dorsal muscles and the proliferation of osteoclasts before heterotopic bone formation. *Biomaterials*, 27(25), pp.4419-4427.

Krupa, P. et al., 2007. Use of 3D geometry modeling of osteochondrosis-like iatrogenic lesions as a template for press-and-fit scaffold seeded with mesenchymal stem cells. *Physiological research / Academia Scientiarum Bohemoslovaca*, 56(1), pp.107-114.

Kruth, J., Leu, M. & Nakagawa, T., 1998. Progress in Additive Manufacturing and Rapid Prototyping. *CIRP Annals - Manufacturing Technology*, 47(2), pp.525-540.

Lacroix, D., Planell, J. & Prendergast, P., 2009. Computer-aided design and finite-element modelling of biomaterial scaffolds for bone tissue engineering. *Philosophical transactions. Series A, Mathematical, physical, and engineering sciences*, 367(1895), pp.1993-2009.

Lam, C.X.F. et al., 2002. Scaffold development using 3D printing with a starch-based polymer. *Materials Science and Engineering C*, 20, pp.49-56.

Leong, K. et al., 2008. Engineering functionally graded tissue engineering scaffolds. *Journal of the mechanical behavior of biomedical materials*, 1(2), pp.140-152.

Lieberman, J.R. & Friedlaender, G.E., 2005. *Bone Regeneration and Repair* 1st ed., Humana Press.

Mackie, E.J. et al., 2008. Endochondral ossification: how cartilage is converted into bone in the developing skeleton. *The international journal of biochemistry & cell biology*, 40(1), pp.46-62.

Maniatopoulos, C., Sodek, J. & Melcher, H., 1988. Bone formation in vitro by stromal cells obtained from bone marrow of young adult rats. *Cell and tissue research*, 254(2), pp.317-330.

Navarro, M. et al., 2008. Biomaterials in orthopaedics. *Journal of the Royal Society, Interface / the Royal Society*, 5(27), pp.1137-1158.

Perera, F.H. et al., 2010. Clarifying the effect of sintering conditions on the microstructure and mechanical properties of β-tricalcium phosphate. *Ceramics International*, 36(6), pp.1929-1935.

Proveti, J.R.C. & Michot, G., 2006. The Brazilian test: a tool for measuring the toughness of a material and its brittle to ductile transition. *International Journal of Fracture*, 139(3-4), pp.455-460.

Ralston, S.H., 2008. Pathogenesis of Paget's disease of bone. *Bone*, 43(5), pp.819-825.

Ralston, S.H., 2005. Structure and metabolism of bone. *Medicine*, 33(12), pp.58-60.

Ramay, H.R.R. & Zhang, M., 2004. Biphasic calcium phosphate nanocomposite porous scaffolds for load-bearing bone tissue engineering. *Biomaterials*, 25, pp.5171-5180.

Ratner, B.D. et al., 2004. *Biomaterials science - An Introduction to Materials in Medicine* 2nd ed., Elsevier Academic Press.

Ribeiro, G. et al., 2011. Novel method to produce β-TCP scaffolds. *Materials Letters*, 65(2), pp.275-277.

Ribeiro, M. et al., 2009. Development of a new chitosan hydrogel for wound dressing. *Wound repair and regeneration : official publication of the Wound Healing Society [and] the European Tissue Repair Society*, 17(6), pp.817-824.

Schindeler, A. et al., 2008. Bone remodeling during fracture repair: The cellular picture. *Seminars in cell & developmental biology*, 19(5), pp.459-466.

Seitz, H. et al., 2009. Different Calcium Phosphate Granules for 3-D Printing of Bone Tissue Engineering Scaffolds. *Advanced Engineering Materials*, 11(5), pp.41-46.

Sikavitsas, V.I. et al., 2003. Mineralized matrix deposition by marrow stromal osteoblasts in 3D perfusion culture increases with increasing fluid shear forces. *Proceedings of the National Academy of Sciences of the United States of America*, 100(25), pp.14683-14688.

Slósarczyk, A. et al., 1997. The FTIR spectroscopy and QXRD studies of calcium phosphate based materials produced from the powder precursors with different Ca/P ratios. *Ceramics International*, 23(4), pp.297-304.

Stewart, G., 2004. *The Skeletal and Muscular Systems* 1st ed., Infobase Publishing.

Sturm, S. et al., 2010. On stiffness of scaffolds for bone tissue engineering-a numerical study. *Journal of biomechanics*, 43(9), pp.1738-1744.

Sun, W. & Lal, P., 2002. Recent development on computer aided tissue engineering--a review. *Computer methods and programs in biomedicine*, 67(2), pp.85-103.

Tate, P., 2008. *Seeley's Principles of Anatomy & Physiology* 1st ed., McGraw-Hill Science/Engineering/Math.

Van der Stok, J. et al., 2010. Bone substitutes in the Netherlands - A systematic literature review. *Acta biomaterialia*.

Wang, C., Wang, W. & Lin, M., 2010. Computers in Industry STL rapid prototyping bio-CAD model for CT medical image segmentation. *Computers in Industry*, 61(3), pp.187-197.

Wen, D. et al., 2010. Lipids and collagen matrix restrict the hydraulic permeability within the porous compartment of adult cortical bone. *Annals of biomedical engineering*, 38(3), pp.558-569.

Whyte, M.P. & Thakker, R.V., 2009. Rickets and osteomalacia. *Medicine*, 37(9), pp.483-488.

Williams, J.M. et al., 2005. Bone tissue engineering using polycaprolactone scaffolds fabricated via selective laser sintering. *Biomaterials*, 26(23), pp.4817-4827.

Yan, X., 1996. A review of rapid prototyping technologies and systems. *Computer-Aided Design*, 28(4), pp.307-318.